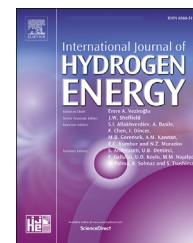


Available online at www.sciencedirect.com

ScienceDirect

journal homepage: www.elsevier.com/locate/ije

DFT study on the oxygen titanium porphyrin as sustainable cyclic catalyst for water splitting

Hong-Xia Yu ^a, Hui-Min Mu ^a, Dong-Ran Zhu ^a, Yong Zhang ^b,
Xiao-Chun Wang ^{a,*}, Sean Xiao-An Zhang ^c

^a Institute of Atomic and Molecular Physics, Jilin University, Changchun, 130012, China

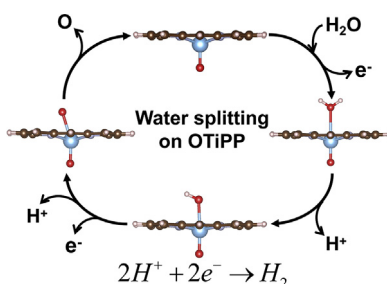
^b Department of Electrical and Computer Engineering, Energy Production and Infrastructure Center, The University of North Carolina at Charlotte, Charlotte, NC, 28223-0001, USA

^c State Key Laboratory of Supramolecular Structure and Materials, Jilin University, Changchun 130012, China

HIGHLIGHTS

- The TiPP can efficiently catalyze the H₂O splitting to form the stable OTiPP.
- The OTiPP is the high-efficiency and recycled catalyst for H₂O splitting.
- The potential barrier transfer effect is the point for the OTiPP catalytic progress.

GRAPHICAL ABSTRACT



ARTICLE INFO

Article history:

Received 24 December 2018

Received in revised form

16 May 2019

Accepted 29 May 2019

Available online 21 June 2019

Keywords:

Oxygen-titanium-porphyrin

Catalysis

Water splitting

Density functional theory

ABSTRACT

With global resource shortage and deterioration of ecological environment, the research and development of clean and renewable energy is of vital importance. Using first-principles calculations, we firstly study water splitting catalyzed by metal based biomolecule porphyrin (MPP) (M = Mg, Ba, Sc, Ti, V, Cr, Mn, Fe, Co, Ni, Cu, and Zn). Among all the systems, after releasing electron, TiPP is the most effective catalyst for H₂O splitting. TiPP and the remainder O atom form the very stable structure OTiPP. The H₂O + OTiPP can release electron with the 6.76 eV potential barrier. The releasing electron process of porphyrin can be easily realized under the effect of solar energy by experiment study. After releasing electron, OTiPP can effectively catalyze the dissociation of H⁺ from H₂O in an exothermic process. The desorption of O atom is an endothermic process with 0.72 eV barrier. The H₂O + OTiPP system can readily return to its original state OTiPP, in other word, the OTiPP can be a sustainable cycling catalyst for water splitting under the effect of potential barrier transfer. The whole catalytic process is remarkable clean without any pollution. This method may open up new avenues for the development of future clean energy and extraordinary biomimetic photosynthesizers.

© 2019 Hydrogen Energy Publications LLC. Published by Elsevier Ltd. All rights reserved.

* Corresponding author.

E-mail address: wangxiaochun@jlu.edu.cn (X.-C. Wang).

<https://doi.org/10.1016/j.ijhydene.2019.05.226>

0360-3199/© 2019 Hydrogen Energy Publications LLC. Published by Elsevier Ltd. All rights reserved.

Introduction

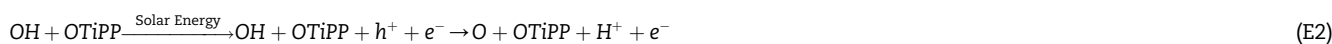
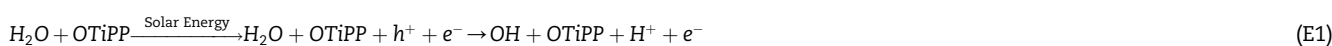
The demand for energy is in a sharp increase with the growth of population and the development of industrialization. The research and development of clean and renewable energy is of vital importance.

To produce ecological energy, water is an ideal resource which can be renewed through its own circulation process. Hydrogen offers the greatest potential benefits of environmental and energy-supply [1]. We can directly get hydrogen from the dissociation of water (via $\text{H}_2\text{O} \rightarrow \text{H}_2 + 1/2\text{O}_2$). However the direct thermal dissociation of water is associated with a large energy barrier requiring temperature in excess of 2000 °C [2]. So it is necessary to seek some catalysts to reduce the reaction barrier. In recent years, there have been several theoretical and experimental studies on Ti-decorated graphene [3,4] and fullerene [5–7] as effective catalysts for water dissociation. Additionally, many other metal catalysts for water dissociation also have been deeply studied, such as gold cluster, metal-embedded nitrogen-doped graphene, rutile (110), goethite (010), ZnO (1010), Ni and Co (100), (110), and (111) surfaces [8–16]. Xinli Kou et al. researched the Ni-Co-Sn alloy as a highly efficient electrocatalyst for water splitting [17]. The NiP₂ nanosheets with interlaced mesh network are designed to split water under alkaline and acid solutions [18]. O-covered Co(0001) surface catalyze water splitting need activation energy 0.967 eV [11]. Shiping Huang et al. used single Ru atom supported on defective grapheme to split water only need a small activation energy of 0.43 eV [19]. These inorganic catalysts have achieved great success, but they rarely realized the complete dissociation of water. In this paper we want to investigate the efficiency of water complete dissociation catalyzed by organic molecule.

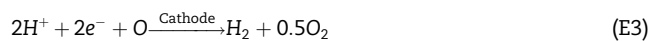
fuel cells and water splitting devices [30]. There also are experimental study about multi-titanium (IV)-porphyrin arrays on the substrate surface as sensitive ultrathin films and theoretical study about titanium-porphyrin as catalyst for direct decomposition of N₂O [31,32]. Inspired by photosynthesis, we want to find highly active and cost-effective catalytic materials to produce hydrogen from water for the clean energy.

In this study, using DFT calculations, we have extensively investigated the potential of water dissociation catalyzed by the metal porphyrin macrocycles (MPP) (M = Mg, Ba, Sc, Ti, V, Cr, Mn, Fe, Co, Ni, Cu, and Zn) at neutral state and at the state releasing one electron per porphyrin macrocycle (MPP⁺). The MPP⁺ systems can be achieved through the effect of solar energy, just like the phenomenon happened in Zn porphyrin [27,28]. The results show that the TiPP system is the best catalysts for the splitting of H among these systems. The desorption of O atom from the TiPP is difficult, so we can get a stable structure of O-Ti-porphyrin macrocycle (OTiPP). Then the dissociation of H₂O catalyzed by OTiPP is investigated. It is found that the dissociation of each H⁺ is also exothermic reaction process, and the desorption of the remaining O atom only needs little energy, which undoubtedly indicates that OTiPP is a perfect catalyst for water splitting via electrons releasing.

The H₂O splitting process catalyzed by OTiPP is shown in equations (E1), (E2) and (E3). Electron and hole would be generated firstly after UV light irradiation. Then H becomes H⁺ by capturing photoinduced hole and then H⁺ is split from H₂O. The catalyst OTiPP needs external energy, such as solar energy, to release electron. Through the effect of potential barrier transfer, the total reaction process of H₂O completely splitting only needs little energy.



Among clean renewable energy resources, solar energy is by far the largest exploitable resource, providing more energy in 1 h to the earth than all of the energy consumed by humans in an entire year [20]. Some studies have explored the efficient photocatalytic hydrogen production from water splitting [21,22]. In Ibrahim Dincer et al.'s study the performance of photo-electro-chemical water-splitting reactor designs for hydrogen production was researched in detail [23]. So far we known that biomolecule porphyrin plays an important role in photosynthesis, because it possesses good chromophore activities over the solar spectrum and excellent electron contributing characteristic (i.e. releasing electrons) due to their large π -electron systems [24–27]. Some papers have demonstrated that Zn porphyrin tends to release electrons under the effect of solar energy at 388 or at 480–505 nm light [27–29]. It has been experimentally proved that cobalt porphyrins as the active centers are proper candidate for acidic



Computational methods

The calculations were performed based on spin-polarized density functional theory (DFT) utilizing the Vienna ab initial Simulation Package (VASP) [33–35] within the projector-augmented wave representation. The exchange-correlation potential was treated at the generalize gradient approximation (GGA) using the Perdew–Burke–Ernzerhof (PBE) functional [36]. Semiempirical corrections accounting for van der Waals (vdW) interactions were described by DFT-D3 method with Becke-Jonson damping. For all calculations the cutoff energy for the plane wave basis set is 520 eV. The k-point mesh was set to $3 \times 3 \times 1$ for the first Brillouin zone. In order to

calculate molecule in periodic boundary condition, the size of the supercell is set to $15 \text{ \AA} \times 15 \text{ \AA} \times 15 \text{ \AA}$ which makes a large vacuum region to avoid the interaction between the neighbor molecules. Gaussian smearing with a width of $\sigma = 0.05 \text{ eV}$ is used in all calculations [9]. The spin polarization and the dipole moment corrections have been considered. The MPP^+ (releasing one electron per porphyrin macrocycle) system is achieved by controlling the total number of electrons in one porphyrin macrocycle. The energy of H ion can be gained by the nonlinear curve fit based on the energies of H atom with different electrons. Geometry optimization was performed on all structures to minimize the Hellmann–Feynman forces with a tolerance of 0.02 eV/\AA . The criterion of energy convergence was set to $1 \times 10^{-5} \text{ eV}$. The optimized titanium porphyrin (TiPP) is close to plane for the $\angle \text{N}_{\text{por}}\text{-Ti-N}_{\text{por}}$ angle is 178° . The Ti–N band length is 2.07 \AA . These results are consistent with the previous works [32,37].

Results and discussion

The H_2O dissociation catalyzed by MPP

Firstly, utilizing the energy minimization theory, we optimize the structure of free water molecule (Fig. 1a). The length of the H–O bond is 0.97 \AA and the H–O–H angle is 104.47° , which is identical to the theoretical values of 0.97 \AA and 104.7° , and the experimental values of 0.95 \AA and 104.50° , respectively [38,39]. From above results, the conclusion can be drawn that the calculation method for water molecule in this work is accurate enough.

Then, we explore the dissociation of the H_2O molecule adsorbed on the top of MPP ($\text{M} = \text{Mg, Ba, Sc, Ti, V, Cr, Mn, Fe, Co, Ni, Cu, and Zn}$) at charge neutrality state ($\text{H}_2\text{O} + \text{MPP}$), or at the state releasing electron ($\text{H}_2\text{O} + \text{MPP}^+$). In order to get the most stable geometry structure three initial inequivalent configurations of H_2O adsorbed on MPP system are taken into account for each of MPP states. H_2O molecule stands right above metal atom in porphyrin macrocycle with three different orientations: first, the plane determined by H and O atoms in H_2O molecule is parallel to the MPP as shown in Fig. 1b; secondly, the plane is perpendicular to the MPP with the O atom pointing away or towards the MPP, as shown in Fig. 1c, d respectively.

The dissociation energy of the first H atom separating from H_2O on the MPP is defined as

$$E_d = (E_{\text{OH}+\text{MPP}} + E_{\text{H}}) - E_{\text{H}_2\text{O}+\text{MPP}} \quad (\text{E4})$$

where $E_{\text{OH}+\text{MPP}}$ and $E_{\text{H}_2\text{O}+\text{MPP}}$ are the energies of the relaxed OH + MPP system and $\text{H}_2\text{O} + \text{MPP}$ system, respectively, and E_{H} is the energy of a free H atom.

The dissociation energy of the first H^+ separating from H_2O on the MPP^+ is defined as

$$E_d = (E_{\text{OH}+\text{MPP}} + E_{\text{H}^+}) - E_{\text{H}_2\text{O}+\text{MPP}^+} \quad (\text{E5})$$

where $E_{\text{OH}+\text{MPP}}$ and $E_{\text{H}_2\text{O}+\text{MPP}^+}$ are the energies of the relaxed OH + MPP and $\text{H}_2\text{O} + \text{MPP}^+$ systems, respectively, and E_{H^+} is the energy of free H^+ . The H^+ will be dissociated from the adsorbed H_2O and then recombine with the released electron to form H atom.

The needed energy of $\text{H}_2\text{O} + \text{MPP}$ releasing electron to form the $\text{H}_2\text{O} + \text{MPP}^+$ state is 4.97 eV that can be gained from solar energy based on the solar harvest property of porphyrin, which is similar with the releasing electron phenomenon [24–27]. Similarly the dissociation energy for each reaction process is defined as the difference between the total energies of the resultants and the reactant. With this definition, a negative value of the dissociation energy represents an exothermic reaction process.

After full optimizing we get the stable configurations of MPP, $\text{H}_2\text{O} + \text{MPP}$, and $\text{H}_2\text{O} + \text{MPP}^+$ systems. We first explore the dissociation of H atom or H ion (H^+) from $\text{H}_2\text{O} + \text{MPP}$ systems and the results show that the dissociation energy of H^+ is lower than that of H atom for each MPP system (Fig. 2). As for the $\text{H}_2\text{O} + \text{MPP}^+$ systems, the similar thing occurs that the splitting of H^+ is easier than H atom. As an example, for the TiPP^+ system, the dissociation energy of H^+ is -2.71 eV , which is much lower than that of H atom (1.65 eV). Thus, we mainly focus on the H^+ dissociation process in the $\text{H}_2\text{O} + \text{MPP}^+$ system. It is exciting that the dissociation energies are negative values which mean that the splitting of H^+ catalyzed by MPP^+ is an exothermic process. All the energies are shown in Fig. 2.

It is obvious that among all the MPP and MPP^+ states the lowest dissociation energy appears in the TiPP^+ system, so we focus on the Ti based biomolecule porphyrin. The dissociation energies of the first and second H^+ catalyzed by TiPP^+ system are -2.71 and -1.99 eV , respectively, which means it is very easy for the H^+ splitting. On the contrary, the desorption of O atom is extremely difficult with 7.32 eV desorption energy. Therefore, we have got a new stable structure, OTiPP . In the following part, we mainly focus on the water splitting process catalyzed by OTiPP .

The H_2O dissociation catalyzed by OTiPP

Based on the above calculations, it is clear that the MPP at the releasing electron state have high catalytic efficiency. Then we will discuss the dissociation of H_2O molecule catalyzed by the OTiPP^+ system ($\text{H}_2\text{O} + \text{OTiPP}^+$). Similar to the dissociation of H_2O molecule in the $\text{H}_2\text{O} + \text{TiPP}^+$ system, we consider three initial inequivalent configurations of $\text{H}_2\text{O} + \text{OTiPP}^+$ system and obtain the most stable structure after fully optimizing.

The dissociation energy of the first H ion separating from H_2O on the OTiPP^+ is defined as

$$E_d = (E_{\text{OH}+\text{OTiPP}} + E_{\text{H}^+}) - E_{\text{H}_2\text{O}+\text{OTiPP}^+} \quad (\text{E6})$$

where $E_{\text{OH}+\text{OTiPP}}$ and $E_{\text{H}_2\text{O}+\text{OTiPP}^+}$ are the energies of the relaxed OH + OTiPP system and $\text{H}_2\text{O} + \text{OTiPP}^+$ system, respectively, and E_{H^+} is the energy of a free H ion. Based on the calculated dissociation energy, we can estimate the H–O bond dissociation efficiency catalyzed by OTiPP^+ relative to the free water. According to the Arrhenius equation [40,41].

$$S_{\text{TiPP}/\text{free}} = \frac{r_{\text{TiPP}}}{r_{\text{free}}} = \frac{A_{\text{TiPP}} e^{-E_{\text{TiPP}}/RT}}{A_{\text{free}} e^{-E_{\text{free}}/RT}} \quad (\text{E7})$$

where r is the bond dissociation rate, A is the interaction (bond dissociation) prefactor and E is the bond dissociation energy. Furthermore, assuming that the prefactors in two conditions are identical ($A_{\text{TiPP}}/A_{\text{free}} = 1$) and the room temperature T is 300 K .

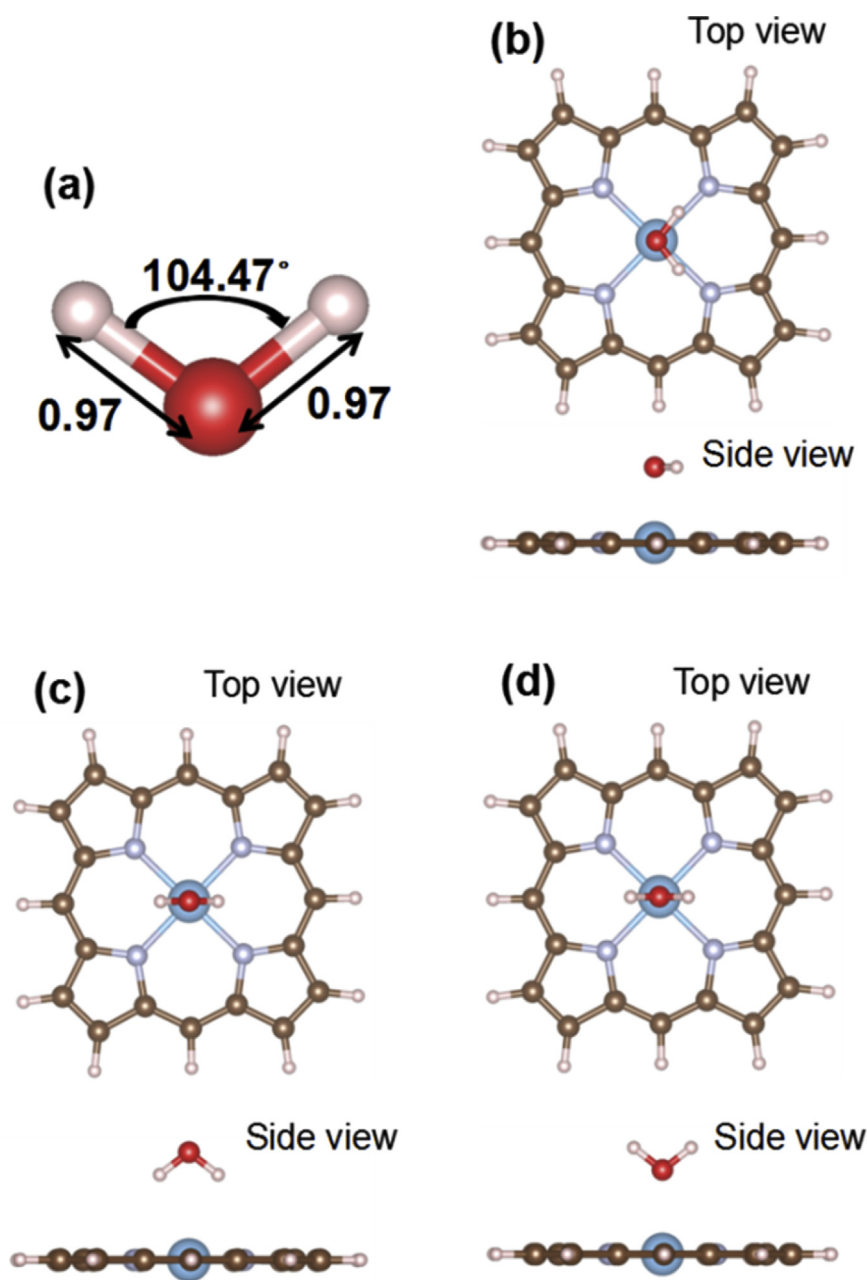


Fig. 1 – The structure of free water (a); the initial geometries of H_2O molecule adsorbed on metal porphyrin macrocycle (MPP) ($M = \text{Mg, Ba, Sc, Ti, V, Cr, Mn, Fe, Co, Ni, Cu, and Zn}$). (b) The plane of H_2O molecule is parallel to the substrate; (c) and (d) the plane of H_2O molecule is perpendicular to the substrate with the O atom pointing away or towards the MPP respectively. Distances are in angstrom (Å). Carbon, hydrogen, nitrogen, oxygen and metal atoms are denoted with brown, white, silvery, red, and blue balls, respectively. (For interpretation of the references to colour in this figure legend, the reader is referred to the Web version of this article).

The dissociation energies of the first and second H^+ as well as the O atom are shown in Table 1. Besides, Table 1 also gives the H-O bond dissociation efficiency catalyzed by OTiPP^+ relative to the free water. It is clear that the H^+ dissociation is an exothermic reaction process catalyzed by OTiPP^+ which leads to a high H-O bond dissociation efficiency. The necessary energy for the desorption of O atom is 0.72eV, much lower than the total energy released in the dissociation process of the first and second H ion (2.38 eV). Therefore, the OTiPP can

catalyze H_2O splitting into H and O atoms and then return to original state OTiPP without any other byproduct, so all the catalytic processes are pure clean.

In order to analyze the catalytic mechanism we plot the Bader charge analysis [42–44] combining three dimensional spin polarized charge distributions of the H_2O , OTiPP^+ ($0 \mu_B$), and $\text{H}_2\text{O} + \text{OTiPP}^+$ system ($1.0 \mu_B$) as shown in Fig. 3, which helps to analyze the charge transfer between the H_2O molecule and the OTiPP . Basically, the charge distribution for every

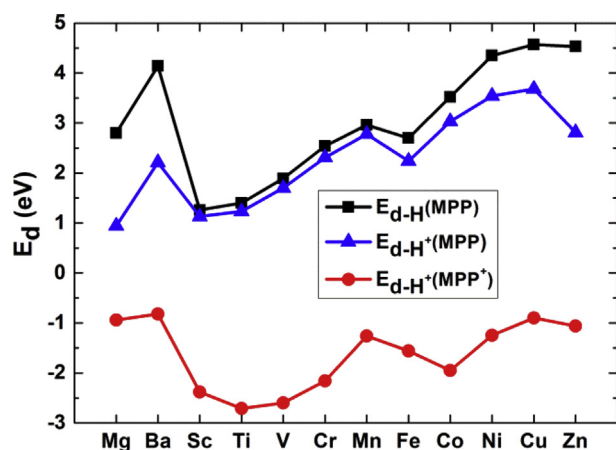


Fig. 2 – Dissociation energy diagrams of H atom and ion splitting from $\text{H}_2\text{O} + \text{MPP}$ systems and H^+ splitting from $\text{H}_2\text{O} + \text{MPP}^+$ systems (M = Mg, Ba, Sc, Ti, V, Cr, Mn, Fe, Co, Ni, Cu, and Zn).

Table 1 – The dissociation energies for the H^+ or O atom (E_d) and the speed of H-O bond dissociation (S). All energies are in eV.

	H_2O	$\text{H}_2\text{O} + \text{OTiPP}^+$	$\text{OH} + \text{OTiPP}^+$	$\text{O} + \text{OTiPP}$
E_d	6.01	-1.01	-1.37	0.72
S	1	10^{121}	10^{128}	

system is in good agreement with the electronegativity of O, N, C, H and Ti atoms which are 3.44, 3.04, 2.55, 2.20 and 1.54, respectively according to Pauling scale [45]. From statistic analysis we can know that for Fig. 3c the total electrons of Ti, N and inner-ring C atoms decrease 0.3e compared with Fig. 3b, while the total electrons of outer-ring C and H atoms increase 0.32e compared with Fig. 3b. The electrons of O_1 do not have any change. In Fig. 3c H13 and H14 atoms become more positive and O_2 atom is more negative after H_2O molecule adsorbed on the OTiPP^+ system compared with Fig. 3a, which makes the polarity of H-O bonds are stronger than that in the free water. The interaction between O_2 atom and OTiPP strengthened because of the electrons redistribution. The effective electrons of H13 and H14 reduced 0.09e, so the H^+ can be dissociated easily from H_2O molecule.

In order to gain more insight into the interaction between water and OTiPP , we have also studied the spin-polarized density of states. Fig. 4 shows the total DOS of the $\text{H}_2\text{O} + \text{OTiPP}^+$ system and the spin-polarized PDOS of the Ti, O_1 , O_2 and H14 atoms in the neighborhood of the Fermi level ($E_F = 0$ eV). In Fig. 4, we can see that the total density of states is asymmetric especially near the Fermi level. This phenomenon suggests a magnetic moment, which is consistent with the three dimensional spin polarized charge density map of the $\text{H}_2\text{O} + \text{OTiPP}^+$ system (Fig. 3b).

The Ti 3d orbit is strongly hybridized with the O_1 2p orbit at the energy range between approximate -0.5 and -1.5 eV, which contributes to the stability of OTiPP . The hybridization between the Ti 3d and O_2 2p orbits locate at -2.5 eV and -1.0 to -1.5 eV. The interaction between Ti and O_1 is stronger

overall than that between Ti and O_2 , and this is consistent with the bond length of Ti and two O atoms. There is a high hybridized peak at -4.5eV between O_2 and H14 atoms, furthermore almost every peak of O_2 and H14 appears in the same energy region. There are some small peaks of hybrid orbitals among the Ti 3d, O_2 2p and H14 1s, which locate at the -2.5 and -3.5 eV energy levels. This means that after the adsorption of H_2O on the OTiPP , Ti atom affects the electron and molecular structure of H_2O , and the electronic state of H_2O changed.

After the dissociation of the first H^+ , OH is left on the OTiPP to form the $\text{OH} + \text{OTiPP}$ system in neutral state. Because of the effect of the surroundings, $\text{OH} + \text{OTiPP}$ will release electron, which will give rise to the redistribution of electrons and change the configurations. In Fig. 5 we show the Bader charge analysis combining three-dimensional spin polarized charge distributions of $\text{OH} + \text{OTiPP}^+$ ($0 \mu_B$) and $\text{O} + \text{OTiPP}$ ($2.0 \mu_B$). In Fig. 5a, the H13- O_2 bond length is 0.976 Å longer than that of free water and the O_2 -Ti bond length is 2.13 Å much shorter than that in Fig. 3c by 0.5 Å. These changes of configurations mean the strong interaction between O_2 and Ti atoms and weak interaction between O_2 and H13 atoms. Therefore, the H13 will be split effortlessly. All these H^+ split from the water molecule can combine with the electrons released from the porphyrin macrocycle substrates to form H atoms. Then two H atoms will combine and form H_2 , which can be used as the clean energy material.

In the final part, we explore the desorption of O atom. The desorption energy of O_2 atom is only 0.72 eV. The configuration and charge distributions are shown in Fig. 5b. It is clear that O_1 and O_2 atom do not located symmetrically at the two side of the substrate. The O_1 atom has strong interaction with Ti atom deduced from the short O_1 -Ti bond length and the strong polarity of O_1 -Ti bond. On the contrary, the O_2 -Ti bond length is much longer and the polarity of O_2 -Ti bond is weaker than that of O_1 -Ti bond. Under the magnetic interaction the O_2 atom moved sidelong. These facts make the desorption of O_2 atom merely need 0.72 eV energy.

The total energy released in the dissociation process of the first and second H ion catalyzed by OTiPP^+ system is 2.38 eV (Table 1). The chemical reactions of water splitting usually take place in liquid water. The free H ion that is split from $\text{H}_2\text{O} + \text{OTiPP}$ can capture the released electron and reduces to $1/2\text{H}_2$ at the interface of the cathode/electrolyte [46], which releases 0.87 eV/atom energy. The two H atoms can combine and form H_2 molecule, which releases 4.53 eV/molecule energy. These released energies are larger than the desorption energy 0.72 eV of O_2 atom from the $\text{O} + \text{OTiPP}$ system. In this case, the desorption of O_2 atom from the $\text{O} + \text{OTiPP}$ system becomes a vital effortless process. All in all, the OTiPP can catalyze one H_2O splitting into H_2 molecule and O atom and then return to original state OTiPP without any other byproduct, so all the catalyzed processes are pure clean.

The reaction path for the splitting of the water molecule on OTiPP is shown in Fig. 6. Splitting the first and second H ions from the water molecule on OTiPP^+ are exothermic reactions with releasing energy of 1.01 and 1.37 eV, respectively. The releasing electrons progresses for $\text{H}_2\text{O} + \text{OTiPP}$ and $\text{OH} + \text{OTiPP}$ are endothermic reactions with the 6.76 and 6.97 eV potential barriers. These

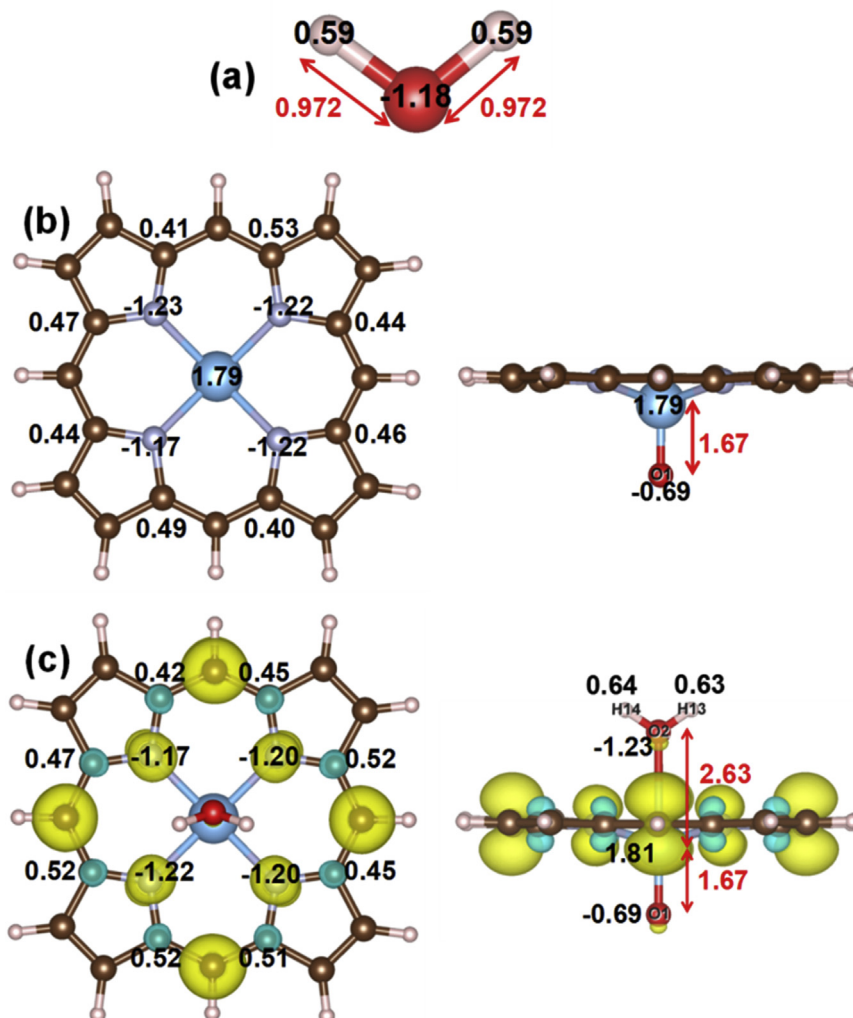


Fig. 3 – The Bader charge analysis combining three-dimensional spin polarized charge distributions. (a) H_2O . (b) OTiPP^+ ($0 \mu_B$) system (c) $\text{H}_2\text{O} + \text{OTiPP}^+$ ($1.0 \mu_B$) system. The O-Ti bond length is marked in red color. The yellow and blue colors indicate the spin-up and spin-down electronic state, respectively. The isosurface value is set to 0.0025 e/Bohr^3 . Distances are in angstrom(\AA). Carbon, hydrogen, nitrogen, oxygen and titanium atoms are denoted with brown, white, silvery, red, and blue balls, respectively. (For interpretation of the references to colour in this figure legend, the reader is referred to the Web version of this article).

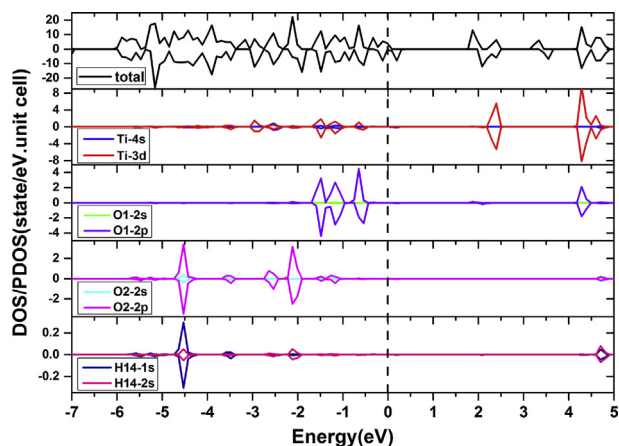


Fig. 4 – The total DOS for $\text{H}_2\text{O} + \text{OTiPP}^+$ system, and PDOS for Ti, O₁, O₂ and H14 atoms, respectively. The Fermi level is set to energy zero.

necessary energies of releasing electrons from porphyrin can be easily obtained from solar energy in experiment [24–27]. The most important fact is that the desorption of remnant O_2 atom from the porphyrin substrate is extremely effortless with only 0.72 eV energy and the porphyrin substrate returns to its original state OTiPP that is ready for the next catalytic reaction.

Using HSE06 methods [47], the linear optical properties of OTiPP are calculated. The absorption coefficient is shown in Fig. 7. Releasing the first electron needs energy 6.76 eV (corresponding 186 nm light) which locates near the absorption peak corresponding absorption coefficient 53000 cm^{-1} . The releasing second electron process needs 6.97 eV (corresponding 178 nm light), and the corresponding absorption coefficient is 21000 cm^{-1} . These two absorption coefficient values mean that the processes of releasing electron can be realized by absorbing solar energy. In experiment, the absorption coefficient peaks can be redshifted by adding some

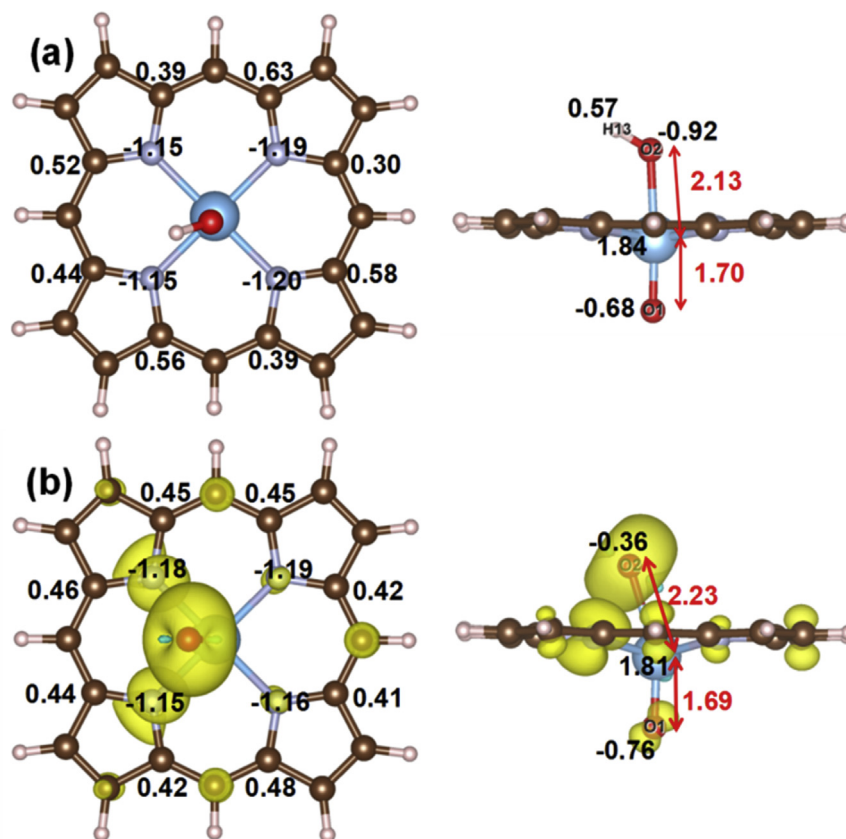


Fig. 5 – The Bader charge analysis combining three-dimensional spin polarized charge distributions. (a) $\text{OH} + \text{OTiPP}^+$ ($0 \mu_B$) system. (b) $\text{O} + \text{OTiPP}$ ($2.0 \mu_B$) system. The O-Ti bond length is marked in red color. The yellow and blue colors indicate the spin-up and spin-down electronic states, respectively. The isosurface value is set to 0.0025 e/Bohr^3 . Distances are in angstrom (Å). Carbon, hydrogen, nitrogen, oxygen and titanium atoms are denoted with brown, white, silvery, red, and blue balls, respectively. (For interpretation of the references to colour in this figure legend, the reader is referred to the Web version of this article).

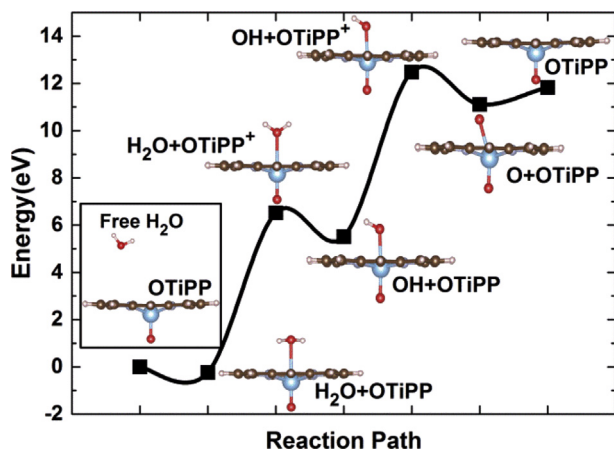


Fig. 6 – The energy variation in the reaction path for the splitting of the water molecule on OTiPP. The inserts show the atomic configurations along the reaction path. The total energy of free water and OTiPP is set to 0 eV . Carbon, hydrogen, nitrogen, oxygen and titanium atoms are denoted with brown, white, silvery, red, and blue balls, respectively. (For interpretation of the references to colour in this figure legend, the reader is referred to the Web version of this article).

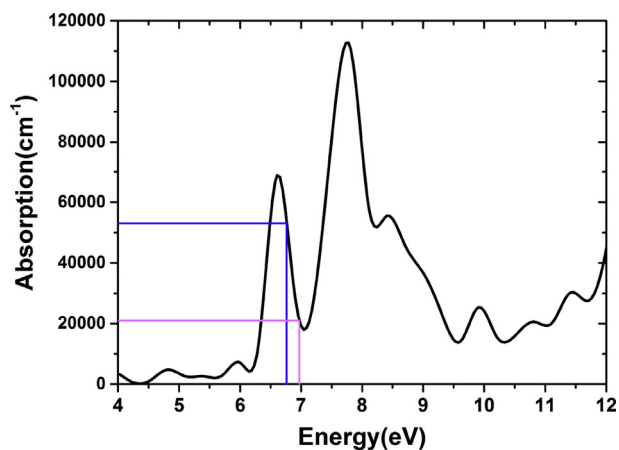


Fig. 7 – Absorption spectra for OTiPP, the value corresponding 6.76 eV are marked by the blue line, the value corresponding 6.97 eV are marked by the pink line. (For interpretation of the references to colour in this figure legend, the reader is referred to the Web version of this article).

functional groups on the TiPP, which makes the releasing electron process easier.

The highest potential barrier appears in the releasing electron process instead of the water splitting process. Overcoming the former potential barrier can be easily realized by solar energy in experiment, and the latter potential barrier becomes remarkably small. This phenomenon can be regarded as the effect of potential barrier transfer. We have provided the OTiPP as a sustainable cyclic catalyst that can split water completely under the effect of potential barrier transfer.

Conclusions

A systematic study on the dissociation energy of H₂O molecule catalyzed by MPP and OTiPP has been conducted to seek a best way of water splitting utilizing first-principles DFT calculations. Our calculations have firstly proved that the first H⁺ of H₂O can be split from TiPP⁺ in a higher efficiency than other MPP and MPP⁺ systems. But the remaining O atom will firmly bond with the Ti atom, to form a very stable OTiPP system. Under external stimuli, the catalyst OTiPP can release electron, which will help to split one H₂O molecule into H₂ molecule and O atom. Results hereon indicate firmly that under the effect of potential barrier transfer, the OTiPP system is thus far the best catalysts for water dissociation among all the above systems. There is one point must be emphasized that in order to release electron to keep the sustainable cyclic catalytic process, the systems need the injection energy which can be easily obtained from the solar energy. It is worth to reemphasize that the whole process of forming OTiPP system and splitting H₂O on the OTiPP system only need H₂O and TiPP without any side-material, and the final products are H₂ and O only. Thus, this fact ensures that the whole catalytic process is remarkable clean without any pollution and the OTiPP can return to original state which means it can be sustainably recycled. This study will be helpful in producing clean energy and finding effective catalysts for the splitting of H₂O or other oxide molecules such as CO₂ and SO₂. Besides, this method may open up new avenues for the development of artificial photo-synthesizers, biomimetic materials, etc.

Acknowledgements

This work was supported by the National Natural Science Foundation of China (Grant No. 11474123, 51373068, 51303063), the program of Chang Jiang Scholars and Innovative Research Team in the University (IRT101713018), and the Natural Science Foundation of Jilin Province of China (Grant No. 20170101154JC). YZ thanks the support of Bissell Distinguished Professorship at UNC-Charlotte.

REFERENCES

- [1] Ogden JM. Hydrogen: the fuel of the future? *Phys Today* 2002;55:69–75.
- [2] Turner JA. Sustainable hydrogen production. *Science* 2004;305.
- [3] Rangel E, Ruiz-Chavarria G, Magana LF. Water molecule adsorption on a titanium–graphene system with high metal coverage. *Carbon* 2009;47:531–3.
- [4] Miao M, Shi H, Wang Q, Liu Y. The Ti₄ cluster activates water dissociation on defective graphene. *Phys Chem Chem Phys: PCCP* 2014;16:5634–9.
- [5] Xue Y. Dissociation of water on Ti-decorated fullerene clusters. *AIP Adv* 2012;2:012163.
- [6] Liu Y, Huang L, Gubbins KE, Buongiorno Nardelli M. Dissociation of water over Ti-decorated C60. *J Chem Phys* 2010;133:084510.
- [7] Huang L, Liu Y-C, Gubbins KE, Nardelli MB. Ti-decorated C60 as catalyst for hydrogen generation and storage. *Appl Phys Lett* 2010;96:063111.
- [8] Jena NK, Chandrakumar KRS, Ghosh SK. Water dissociation on a gold cluster: the effect of carbon nanostructures as a substrate. *RSC Adv* 2012;2:10262.
- [9] Liu L-L, Chen C-P, Zhao L-S, Wang Y, Wang X-C. Metal-embedded nitrogen-doped graphene for H₂O molecule dissociation. *Carbon* 2017;115:773–80.
- [10] Wen B, Zhang L, Wang D, Lang X. The distribution of excess carriers and their effects on water dissociation on rutile (110) surface. *Comput Mater Sci* 2017;136:150–6.
- [11] Yang J, Ma JJ, Ma SH, Dai XQ. Theoretical study of direct versus oxygen-assisted water dissociation on Co(0 0 0 1) surface. *Chem Phys Lett* 2017;681:29–35.
- [12] Ma FF, Ma SH, Jiao ZY, Dai XQ. Adsorption and decomposition of H₂O on cobalt surfaces: a DFT study. *Appl Surf Sci* 2016;384:10–7.
- [13] Zhang J, Wang T, Liu P, Liao Z, Liu S, Zhuang X, et al. Efficient hydrogen production on MoNi₄ electrocatalysts with fast water dissociation kinetics. *Nat Commun* 2017;8:15437.
- [14] Seenivasan H, Jackson B, Tiwari AK. Water dissociation on Ni(100), Ni(110), and Ni(111) surfaces: reaction path approach to mode selectivity. *J Chem Phys* 2017;146:074705.
- [15] Zhou L, Xiu F, Qiu M, Xia S, Yu L. The adsorption and dissociation of water molecule on goethite (010) surface: a DFT approach. *Appl Surf Sci* 2017;392:760–7.
- [16] Kenmoe S, Biedermann PU. Water aggregation and dissociation on the ZnO(101[combining macron]0) surface. *Phys Chem Chem Phys : PCCP* 2017;19:1466–86.
- [17] Liu Y, Lu H, Kou X. Electrodeposited Ni-Co-Sn alloy as a highly efficient electrocatalyst for water splitting. *Int J Hydrogen Energy* 2019;44:8099–108.
- [18] Cao Q, Wang C, Chen S, Xu X, Liu F, Geng X, et al. Vertically aligned NiP₂ nanosheets with interlaced mesh network for highly efficient water splitting under alkaline and acid solutions. *Int J Hydrogen Energy* 2019;44:6535–43.
- [19] Guo X, Liu S, Huang S. Single Ru atom supported on defective graphene for water splitting: DFT and microkinetic investigation. *Int J Hydrogen Energy* 2018;43:4880–92.
- [20] Lewis NS, Nocera DG. Powering the planet: chemical challenges in solar energy utilization. *Proc Natl Acad Sci USA* 2006;103:15729–35.
- [21] Wang R, Ni S, Liu G, Xu X. Hollow CaTiO₃ cubes modified by La/Cr co-doping for efficient photocatalytic hydrogen production. *Appl Catal B Environ* 2018;225:139–47.
- [22] Zhang Y-C, Li Z, Zhang L, Pan L, Zhang X, Wang L, et al. Role of oxygen vacancies in photocatalytic water oxidation on ceria oxide: experiment and DFT studies. *Appl Catal B Environ* 2018;224:101–8.
- [23] Qureshy AMMI, Ahmed M, Dincer I. Performance assessment study of photo-electro-chemical water-splitting reactor designs for hydrogen production. *Int J Hydrogen Energy* 2019;44:9237–47.

- [24] Ge R, Li X, Kang S-Z, Qin L, Li G. Highly efficient graphene oxide/porphyrin photocatalysts for hydrogen evolution and the interfacial electron transfer. *Appl Catal B Environ* 2016;187:67–74.
- [25] Yamamoto A, Mizuno Y, Teramura K, Hosokawa S, Shishido T, Tanaka T. Visible-light-assisted selective catalytic reduction of NO with NH₃ on porphyrin derivative-modified TiO₂ photocatalysts. *Catal Sci Technol* 2015;5:556–61.
- [26] Chen D, Wang K, Hong W, Zong R, Yao W, Zhu Y. Visible light photoactivity enhancement via CuTCPP hybridized g-C₃N₄ nanocomposite. *Appl Catal B Environ* 2015;166–167:366–73.
- [27] Kim JH, Lee SH, Lee JS, Lee M, Park CB. Zn-containing porphyrin as a biomimetic light-harvesting molecule for biocatalyzed artificial photosynthesis. *Chem Commun* 2011;47:10227–9.
- [28] D'Souza F, Smith PM, Zandler ME, McCarty AL, Ito M, Araki Y, et al. Energy transfer followed by electron transfer in a supramolecular triad composed of boron dipyrin, zinc porphyrin, and fullerene: a model for the photosynthetic antenna-reaction center complex. *J Am Chem Soc* 2004;126:7898–907.
- [29] Li Siy Feirong, Ciringh Yangzhen, Seth Jyoti, Martin Charles H, Singh Deepak L, Kim Dongho, et al. Design, synthesis, and photodynamics of light-harvesting arrays comprised of a porphyrin and one, two, or eight boron-dipyrin accessory pigments. *J Am Chem Soc* 1998;120:10001–17.
- [30] Sohrabi S, Dehghanpour S, Ghalkhani M. A cobalt porphyrin-based metal organic framework/multi-walled carbon nanotube composite electrocatalyst for oxygen reduction and evolution reactions. *J Mater Sci* 2017;53:3624–39.
- [31] He W-L, Fang F, Ma D-M, Chen M, Qian D-J, Liu M. Palladium-directed self-assembly of multi-titanium(IV)-porphyrin arrays on the substrate surface as sensitive ultrathin films for hydrogen peroxide sensing, photocurrent generation, and photochromism of viologen. *Appl Surf Sci* 2018;427:1003–10.
- [32] Maitarad P, Namuangruk S, Zhang D, Shi L, Li H, Huang L, et al. Metal-porphyrin: a potential catalyst for direct decomposition of N(2)O by theoretical reaction mechanism investigation. *Environ Sci Technol* 2014;48:7101–10.
- [33] Zupan A, Burke K, Ernzerhof M, Perdew JP. Distributions and averages of electron density parameters: explaining the effects of gradient corrections. *J Chem Phys* 1997;106:10184–93.
- [34] Rungger I, Sanvito S. Algorithm for the construction of self-energies for electronic transport calculations based on singularity elimination and singular value decomposition. *Phys Rev B* 2008;78.
- [35] Rocha AR, García-Suárez VM, Bailey S, Lambert C, Ferrer J, Sanvito S. Spin and molecular electronics in atomically generated orbital landscapes. *Phys Rev B* 2006;73.
- [36] Hammer B, Hansen LB, Norskov JK. Improved adsorption energetics within density-functional theory using revised Perdew-Burke-Ernzerhof functionals. *Phys Rev B* 1999;59(11):7413–21.
- [37] Maitarad P, Meeprasert J, Shi L, Limtrakul J, Zhang D, Namuangruk S. Mechanistic insight into the selective catalytic reduction of NO by NH₃ over low-valent titanium-porphyrin: a DFT study. *Catal Sci Technol* 2016;6:3878–85.
- [38] Jung J, Shin H-J, Kim Y, Kawai M. Controlling water dissociation on an ultrathin MgO film by tuning film thickness. *Phys Rev B* 2010;82.
- [39] Lide e David R. CRC handbook of chemistry and physics. Boca Raton, FL: CRC Press; 2005. Internet Version 2005.
- [40] Wang X-C, Zhang Y, Liu F-C, Ma Y, Feng W, Zhang SX-A. Dynamic nano-pulling effect of the boron-functionalized graphene monovacancy for molecule dissociation. *J Phys D Appl Phys* 2013;46:385302.
- [41] Li Y, Zhou Z, Shen P, Chen Z. Two-dimensional polyphenylene: experimentally available porous graphene as a hydrogen purification membrane. *Chem Commun* 2010;46:3672–4.
- [42] Henkelman G, Arnaldsson A, Jónsson H. A fast and robust algorithm for Bader decomposition of charge density. *Comput Mater Sci* 2006;36:354–60.
- [43] Tang W, Sanville E, Henkelman G. A grid-based Bader analysis algorithm without lattice bias. *J Phys Condens Matter: Inst Phys J* 2009;21:084204.
- [44] Liu L-L, Wang Y, Chen C-P, Yu H-X, Zhao L-S, Wang X-C. Tuning the electronic and magnetic properties of pentagraphene using a hydrogen atom: a theoretical study. *RSC Adv* 2017;7:40200–7.
- [45] Allred AL. Electronegativity values from thermochemical data. *J Inorg Nucl Chem* 1961;17:215–21.
- [46] Sun J, Zhong DK, Gamelin DR. Composite photoanodes for photoelectrochemical solar water splitting. *Energy Environ Sci* 2010;3:1252.
- [47] Zhao L-S, Wang Y, Chen C-P, Liu L-L, Yu H-X, Zhang Y, et al. Elastic, electronic and optical properties of stable pentagonal ZnO₂. *Phys E Low-dimens Syst Nanostruct* 2017;91:82–7.